CHEMISTRY OF MATERIALS
Article
Cite This: Chem. Mater. 2019, 31, 7238−7247
pubs.acs.org/cm

Materials Compatibility in Rechargeable Aluminum Batteries: Chemical and Electrochemical Properties between Vanadium Pentoxide and Chloroaluminate Ionic Liquids

Xiaoyu Wen,[†] Yuhang Liu,[‡] Ankur Jadhav,[§] Jian Zhang,[∥] Dan Borchardt,[⊥] Jiayan Shi,[†] Bryan M. Wong,[†,∥] Biplab Sanyal,[‡] Robert J. Messinger,[*,§] and Juchen Guo[*,†,∥]

[†]Department of Chemical and Environmental Engineering, University of California—Riverside, Riverside, California 92521, United States

[‡]Department of Physics and Astronomy, Uppsala University, Box-516, 751 20 Uppsala, Sweden

[§]Department of Chemical Engineering, The City College of New York, CUNY, New York, New York 10031, United States

[∥]Materials Science and Engineering Program, University of California—Riverside, Riverside, California 92521, United States

[⊥]Department of Chemistry, University of California—Riverside, Riverside, California 92521, United States

Supporting Information

ABSTRACT: To demonstrate the importance of electrode/electrolyte stability in rechargeable aluminum (Al) batteries, we investigate the chemical compatibility between vanadium pentoxide (V_2O_5), a proposed positive electrode material for Al batteries, and the common chloroaluminate ionic liquid electrolytes. We reveal that V_2O_5 reacts with both the Lewis acidic ($Al_2Cl_7^-$) and the Lewis neutral species ($AlCl_4^-$) within the electrolyte. The reaction products are identified using a combination of electrochemical analyses, Raman spectroscopy, liquid-state and solid-state nuclear magnetic resonance (NMR) spectroscopy, and density functional theory (DFT) calculations. The results establish that V_2O_5 chemically reacts with $Al_2Cl_7^-$ to form vanadium oxychloride ($VOCl_3$) and amorphous aluminum oxide. V_2O_5 also chemically reacts with $AlCl_4^-$ to produce dioxovanadium chloride (VO_2Cl) and a new species of metavanadate anion coordinated with aluminum chloride ($AlCl_3VO_3^-$). These products furthermore exhibit electrochemical redox activity between V^{5+} and V^{2+} oxidation states. Our results have significant implications when interpreting the electrochemical properties and mechanisms of rechargeable Al−V_2O_5 batteries.

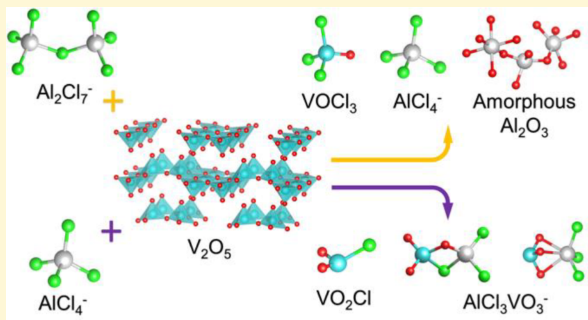

INTRODUCTION

Rechargeable aluminum (Al) batteries have attracted growing attention as a potential alternative to current electrochemical energy storage technologies.[1−3] One of the key challenges in the development of rechargeable Al batteries is the lack of feasible electrolytes that enable reversible Al electrodeposition-stripping at room temperature.[4] The most common electrolytes are chloroaluminate ionic liquids (ILs) (or the bromoaluminate analogues),[5−7] which are deep eutectic solvents composed of aluminum chloride ($AlCl_3$) and organic chloride salts with imidazolium, pyridinium, or ammonium cations.[8−11] These chloroaluminate electrolytes are highly corrosive, corroding even stainless steel.[12] The search for suitable positive electrode materials is another critical challenge facing rechargeable Al batteries. In particular, the trivalent Al^{3+} ion is inherently difficult to intercalate into crystalline host structures due to the strong Coulombic attractions between the highly charged Al^{3+} cations and the host anionic frameworks, which creates high activation energies for solid-state diffusion.[13] The conversion-type materials such as chalcogens including sulfur,[14] selenium,[15] and tellurium[16] were also investigated as potential positive electrodes for rechargeable Al batteries.

Nevertheless, transition metal oxides and sulfides are popular positive electrode materials in reported investigations on Al batteries.[17−24] Among them, vanadium pentoxide (V_2O_5) has received particular attention due to its layered structure and the ability of the V atoms to support a wide range of oxidation states, which could be beneficial for Al^{3+} intercalation.[25−30] However, it is essential to understand the chemical stability of any positive electrode candidate in chloroaluminate IL electrolytes prior to characterizing their electrochemical performance. Electrolyte/electrode chemical stability is a critical property that has been largely overlooked in the literature on rechargeable Al batteries. Therefore, in this study we investigate the chemical stability of V_2O_5 in a typical

Received: April 19, 2019
Revised: August 24, 2019
Published: August 26, 2019

DOI: 10.1021/acs.chemmater.9b01556
Chem. Mater. 2019, 31, 7238−7247

chloroaluminate IL electrolyte, 1-ethyl-3-methylimidazolium aluminum chloride ($AlCl_3$-[EMIm]Cl). The electrolyte contains two chloroaluminate anions, $Al_2Cl_7^-$ and $AlCl_4^-$, which are governed by the chemical equilibria:[31]

$$AlCl_3 + [EMIm]Cl \rightarrow [EMIm]^+ + AlCl_4^- \quad (1)$$

$$AlCl_3 + AlCl_4^- \rightarrow Al_2Cl_7^- \quad (2)$$

We examine the stability of V_2O_5 with respect to each chloroaluminate anion by using electrolyte mixtures of $AlCl_3$/[EMIm]Cl = 2:1 (Lewis acidic, where $Al_2Cl_7^-$ is present as the major anionic species) and $AlCl_3$/[EMIm]Cl = 1:1 (Lewis neutral, where $AlCl_4^-$ is the only anionic species present). We reveal that both chloroaluminate anions chemically react with V_2O_5, and we investigate the nature and electrochemical properties of the reaction products.

■ EXPERIMENTAL SECTION

Synthesis. V_2O_5 was prepared based on a reported method[32] and confirmed by powder X-ray diffraction (XRD) patterns and scanning electron microscopy (SEM) (Figure S1, Supporting Information). The Lewis neutral electrolyte ($AlCl_3$:[EMIm]Cl in a molar ratio of 1:1) was purchased from Sigma-Aldrich and used as received. The Lewis acidic electrolyte ($AlCl_3$:[EMIm]Cl in a molar ratio of 2:1) was prepared by mixing the Lewis neutral electrolyte with anhydrous aluminum chloride ($AlCl_3$, 99.99%, Sigma-Aldrich) in a dried glass vial with a molar ratio of 1:1. The chemical reactions between V_2O_5 and the electrolytes were performed at either room temperature or 70 °C, and all the reactions and electrochemical experiments were performed in an argon-filled glovebox (<1 ppm of H_2O and O_2).

Electrochemical Measurements. Cyclic voltammetry (CV) was carried out in three-electrode cells using a Gamry potentiostat (Reference 3000) with a glassy carbon (GC) working electrode (3 mm disc, Gamry), Al wire (1 mm diameter, 99.9995%, Alfa Aesar) reference electrode, and Al wire coil (2 mm diameter, 99.9995%, Alfa Aesar) counter electrode. All electrodes were polished and cleaned prior to every experiment. Tantalum (Ta) foil (≥99.9%, Sigma-Aldrich) was used as the working electrode in the chronoamperometry experiments. The Ta foil was first washed with acetone for grease removal and then immersed in 2% hydrofluoric acid for 3 days at 80 °C to remove the stable oxide surface layer. The obtained Ta foil was polished consecutively using 1200 and 2400 grit SiC sandpaper, followed by rinsing with an adequate amount of anhydrous ethanol before use.

Raman Spectroscopy. Raman spectra were obtained using a Horiba LabRAM HR with a 785 nm laser source. The samples were sealed in a 3 mm NMR tube under argon and analyzed with 64 scans at a resolution of 4 cm^{-1} and a grating with 600 lines per mm.

NMR Spectroscopy. Liquid-state ^{27}Al and ^{51}V NMR spectra were acquired using a Bruker NEO 400 spectrometer with a 9.4 T narrow-bore superconducting magnet operating at 104.26 and 105.24 MHz for ^{27}Al and ^{51}V nuclei, respectively. All samples were sealed in a 5 mm standard NMR tube, within which an external standard was inserted in a 3 mm NMR tube. All liquid-state ^{27}Al and ^{51}V experiments were conducted with radio frequency field strengths of 20.8 kHz and 20.5 kHz, respectively, which correspond to 90° pulses of 12.0 and 12.2 μs. A recycle delay of 3 s was used for all liquid-state ^{27}Al and ^{51}V experiments. All NMR experiments were conducted at ambient temperature. Liquid-state ^{27}Al and ^{51}V chemical shifts were referenced to 1 M $AlCl_3$ in D_2O (99.9 atom % D, Sigma-Aldrich) and vanadium oxychloride ($VOCl_3$, 99%, Sigma-Aldrich) in benzene-d_6 (C_6D_6, 99.96 atom % D, Sigma-Aldrich) in a volume ratio of 9:1, respectively.

Solid-state ^{27}Al and ^{51}V NMR spectra were acquired on a Bruker AVANCE III 600 NMR spectrometer with a 14.1 T narrow-bore superconducting magnet operating at 156.39 and 157.79 MHz for ^{27}Al and ^{51}V nuclei, respectively. A PhoenixNMR 1.6 mm HXY NB probehead was used with zirconia rotors. All samples were rotated at 40 kHz MAS. To minimize heating due to MAS, dry air at 293.2 K was pumped through the probehead at 600 L h^{-1}. All ^{27}Al and ^{51}V experiments were conducted with radio frequency field strengths of 166 kHz and 156 kHz, respectively, which correspond to 90° pulses of 1.5 and 1.6 μs, respectively. To fully quantify the relative populations of quadrupolar (spin-5/2) ^{27}Al moieties, solid-state ^{27}Al single-pulse experiments were performed using a $\pi/12$ pulse (0.31 μs). Solid-state 1D ^{51}V Hahn-echo MAS spectra were acquired to minimize probe ringdown, where a half-echo delay of one rotor period (25 μs) was used. The solid-state ^{27}Al triple-quantum (3Q)-MAS NMR spectrum was acquired using a 3-pulse sequence using excitation, conversion, and central-transition selective pulses of 4.0 μs, 1.2 μs, and 24 μs, respectively, and a z-filter delay of one rotor period (25 μs). The 2D spectrum was subjected to an isotropic shearing transformation. A recycle delay of 0.1 s was used for all ^{27}Al and ^{51}V experiments. Solid-state ^{27}Al and ^{51}V chemical shifts were referenced to 1 M aqueous solutions of $Al(NO_3)_3$ and $VOCl_3$, respectively.

X-ray Diffraction and X-ray Photoelectron Spectroscopy. The XRD was performed with a PANalytical Empyrean instrument (45 kV/40 mA) with a Cu Kα source. The XRD sample was rinsed with an adequate amount of anhydrous dichloromethane (CH_2Cl_2) to remove the residue of the reactants, followed by drying at 80 °C in a vacuum oven. The sample for solid-state ^{27}Al and ^{51}V NMR was prepared in the same fashion. The X-ray photoelectron spectroscopy (XPS) was conducted with a high sensitivity Kratos AXIS Supra with monochromatic Al Kα radiation (1486.7 eV). The emission current for excitation was 15 mA. All XPS spectra were analyzed by the Casaxps software using the carbon 1s peak at 284.8 eV as the reference. The XPS sample was first rinsed with anhydrous CH_2Cl_2 three times to remove the residue of the reactants and then rinsed with an adequate amount of anhydrous toluene to remove residual CH_2Cl_2 to avoid the interference of the Cl element from CH_2Cl_2. The sample rinsing was performed in an argon-filled glovebox, and the rinsed sample was dried at 80 °C in the glovebox. The XPS samples were transferred and loaded under inert gas continuously without exposure to ambient environment. The surface morphology and elemental composition of samples were studied by SEM and energy dispersive X-ray (EDX) spectroscopy.

Theoretical Calculations. Density functional theory (DFT) calculations of Raman spectra were performed using the VASP package.[33,34] All results were obtained using the projector-augmented plane-wave method[35,36] by explicitly including 5 valence electrons for V atoms, 6 for O, 3 for Al, and 7 for Cl, respectively. A plane-wave cutoff of 700 eV was used in all of our calculations. The exchange-correlation interactions were described with a generalized gradient approximation (GGA) in the form of the Perdew, Burke, and Ernzerhof (PBE) functional.[37] Brillouin zone integrations were performed with a Gaussian broadening of 0.01 eV during all relaxations and self-consistent calculations.[38] A 1 × 1 × 1 Monkhorst−Pack k-point mesh centered at the Gamma point was used to sample the Brillouin Zone.[39] All geometric structures were fully relaxed until the force on each atom was smaller than 10^{-3} eV/Å. The self-consistent electronic loop was stopped when the total energy change was smaller than 10^{-8} eV/ Å. The calculations of phonon frequencies were performed using Phonopy.[40] To calculate the Raman activities and simulate the Raman spectra, the Phonopy-Spectroscopy package was used.[41] The electron localization function (ELF) was calculated to distinguish different bonding interactions in molecules.[42] A Bader analysis was employed to determine the local charge of atoms in the molecules.[43,44]

■ RESULTS AND DISCUSSION

To study the chemical stability between V_2O_5 and the Lewis acidic species $Al_2Cl_7^-$, V_2O_5 was mixed in the Lewis acidic $AlCl_3$-[EMIm]Cl electrolyte (2:1 molar ratio) with a V_2O_5/$AlCl_3$ molar ratio of 0.2:1. The reaction temperature was set at 70 °C to expedite the reaction to complete within a few hours. V_2O_5 was observed to completely dissolve in the electrolyte, and precipitate subsequently formed from the solution (Figure

DOI: 10.1021/acs.chemmater.9b01556
Chem. Mater. 2019, 31, 7238−7247

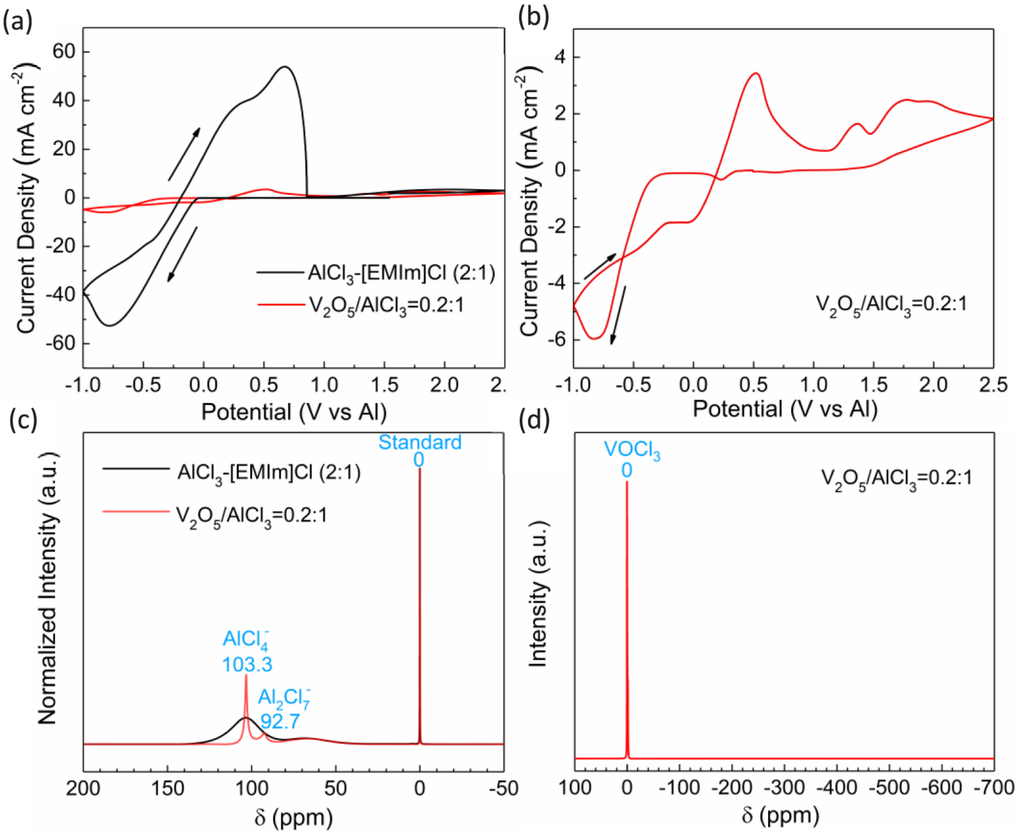

Figure 1. (a) CV scans of the Lewis acidic AlCl$_3$-[EMIm]Cl electrolyte before (black) and after (red) reaction with V_2O_5 at 70 °C; (b) enlarged CV scan after the reaction; and (c) liquid-state ^{27}Al NMR spectra and (d) liquid-state ^{51}V NMR spectrum of the Lewis acidic AlCl$_3$-[EMIm]Cl electrolyte before (black) and after (red) reaction with V_2O_5.

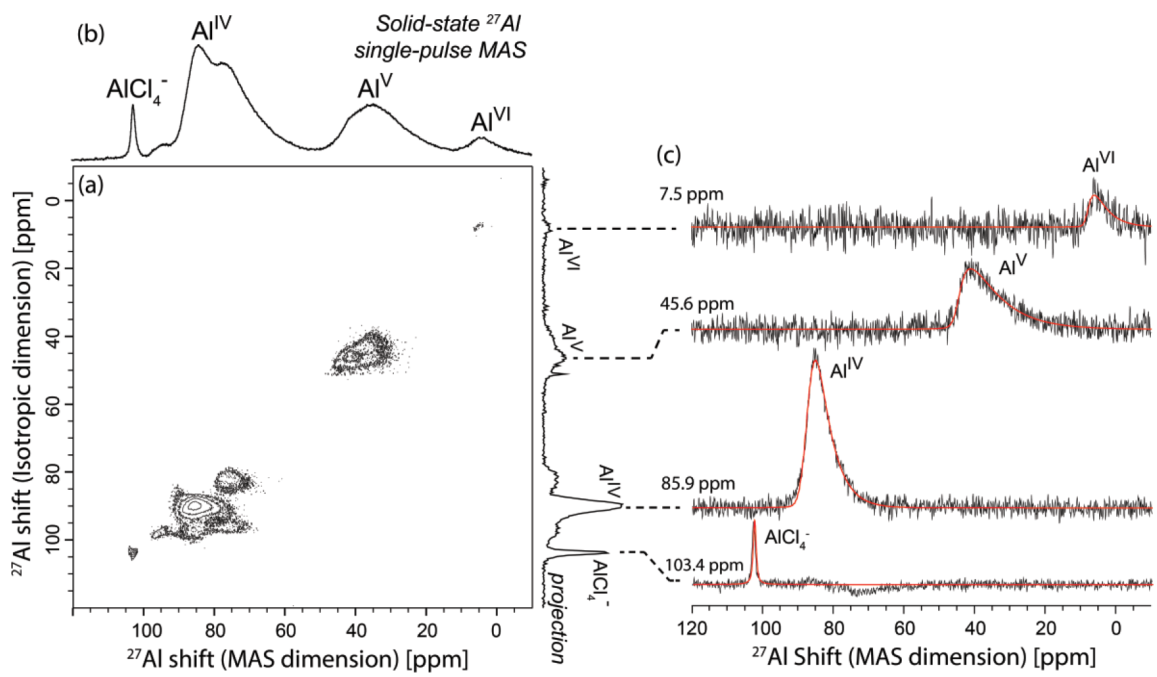

Figure 2. (a) Solid-state 2D ^{27}Al triple-quantum (3Q)-MAS NMR spectrum of the precipitate from the reaction between V_2O_5 and $Al_2Cl_7^-$. A skyline projection of the isotropic dimension is displayed on the vertical axis. (b) A separately acquired quantitative 1D ^{27}Al single-pulse MAS spectrum is displayed along the horizontal axis, where ^{27}Al signals associated with four-, five-, and six-coordinated aluminum moieties are labeled. (c) Selected 1D slices of the MAS dimension (black) were fit to a simplified Czjzek distribution (red), reflecting distributions of chemical shifts and quadrupolar interactions typical of amorphous solids.

DOI: 10.1021/acs.chemmater.9b01556
Chem. Mater. 2019, 31, 7238−7247

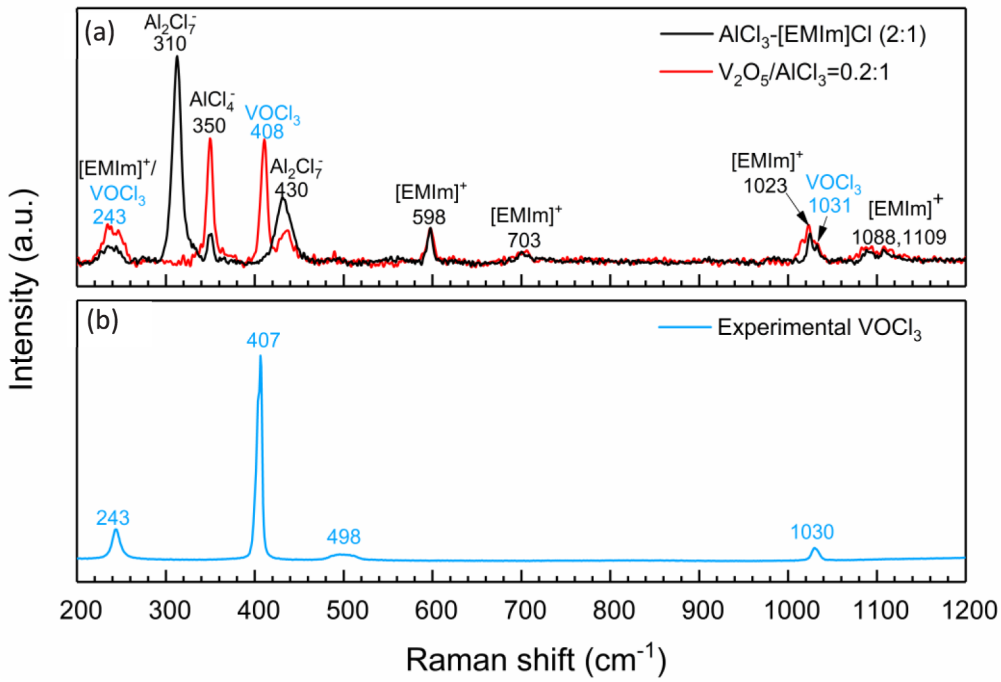

Figure 3. Raman spectra of (a) the Lewis acidic $AlCl_3$-[EMIm]Cl (molar ratio 2:1) electrolyte before (black) and after (red) reaction with V_2O_5 (molar ratio of V_2O_5:$AlCl_3$ = 0.2:1) at 70 °C and (b) Raman spectrum of the commercial $VOCl_3$.

S2, Supporting Information). Figure 1a,b shows the comparison of the CV scans of the Lewis acidic $AlCl_3$-[EMIm]Cl electrolyte before and after the reaction with V_2O_5. The pristine electrolyte clearly demonstrates a pair of redox peaks corresponding to the Al deposition-stripping mechanism according to Reaction 3:[45]

$$4Al_2Cl_7^- + 3e^- \rightleftharpoons Al + 7AlCl_4^- \quad (3)$$

After the reaction with V_2O_5, the CV peaks associated with Al electrodeposition-stripping significantly diminished, which provides strong evidence that the electroactive species $Al_2Cl_7^-$ was consumed by reaction with V_2O_5. This observation is supported by the liquid-state ^{27}Al NMR spectra displayed in Figure 1c. The broad ^{27}Al signal at 103.3 ppm in the spectrum of the pristine $AlCl_3$-[EMIm]Cl electrolyte represents the dynamic exchange between $Al_2Cl_7^-$ and $AlCl_4^-$ according to the equilibrium[27]

$$Al_2Cl_7^- + Cl^- \rightleftharpoons 2AlCl_4^- \quad (4)$$

After the reaction with V_2O_5, the dynamic exchange shown in Reaction 4 slowed significantly due to the presence of additional reaction product, namely, $AlCl_4^-$; thus, the broad NMR peak split into two distinct signals at 103.3 and 92.7 ppm associated with $AlCl_4^-$ and $Al_2Cl_7^-$, respectively. Liquid-state ^{51}V NMR was further performed to identify the V-containing species produced from the reaction. As shown in Figure 1d, a single ^{51}V signal at 0 ppm was observed, which can be unambiguously assigned as $VOCl_3$ based on not only the literature[46,47] but also the ^{51}V NMR spectrum of the commercial $VOCl_3$, which was used as the ^{51}V chemical shift reference. The reaction between V_2O_5 and the Lewis acidic $AlCl_3$-[EMIm]Cl electrolyte can be completed at room temperature with the identical mechanism shown in Figure S3, Supporting Information.

The solid precipitate from the reaction was studied with powder XRD and solid-state NMR. The XRD pattern is featureless (Figure S4, Supporting Information), establishing its amorphous structure. Solid-state 2D ^{27}Al 3Q-MAS and 1D ^{27}Al single-pulse NMR spectra were also acquired on the precipitate (Figure 2a,b, respectively). The ^{27}Al single-pulse NMR spectrum, acquired under quantitative conditions, establishes that the precipitate contains aluminum moieties in three different coordination environments: Al^{IV} (~85 ppm), Al^{V} (~34 ppm), and Al^{VI} (~4 ppm), whose relative populations are 63%, 26%, and 11%, respectively. The ^{27}Al signal at 103.4 ppm is associated with residual $AlCl_4^-$ from the electrolyte. Amorphous solids exhibit local distributions of molecular structures (e.g., bond angles and bond lengths) and, consequently, distributions of electronic environments. The resulting solid-state ^{27}Al NMR spectra thus exhibit distributions of chemical shifts and quadrupolar interactions, and the latter is sensitive to local electric field gradients and broadens the NMR spectra. The 2D ^{27}Al 3Q-MAS spectrum correlates the MAS dimension (horizontal) with an isotropic dimension (vertical) that removes second-order quadrupolar broadening, enhancing resolution. The 1D slices of the different Al coordination environments (Figure 2c) were fit using a simplified Czjzek distribution model (Table S1, Supporting Information), which accounts for Gaussian distributions of isotropic chemical shifts and quadrupolar interactions, establishing that the precipitate exhibits statistical disorder typically observed in amorphous solids (e.g., such as glasses).[48−50] This result further establishes the amorphous nature of the precipitate. In combination, the solid-state ^{27}Al NMR results are consistent with an amorphous aluminum oxide (Al_2O_3) product.[51−53] The solid-state ^{51}V 1D MAS NMR spectrum of the precipitate (Figure S5 in Supporting Information) reveals only residual V_2O_5.

The Lewis acidic $AlCl_3$-[EMIm]Cl electrolyte before and after the reaction with V_2O_5 was also characterized with Raman spectroscopy. As displayed in Figure 3a (black curve), besides the peaks indexed to the $[EMIm]^+$ cation, the peaks at 310 and

DOI: 10.1021/acs.chemmater.9b01556
Chem. Mater. 2019, 31, 7238−7247

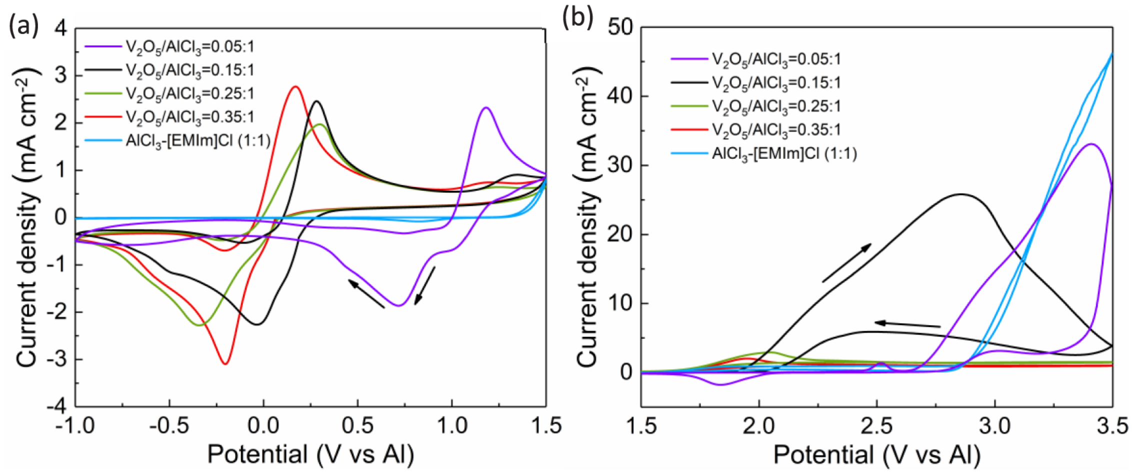

Figure 4. CV scans of the Lewis neutral $AlCl_3$-[EMIm]Cl electrolyte before and after reaction with V_2O_5 at different $V_2O_5/AlCl_3$ molar ratios.

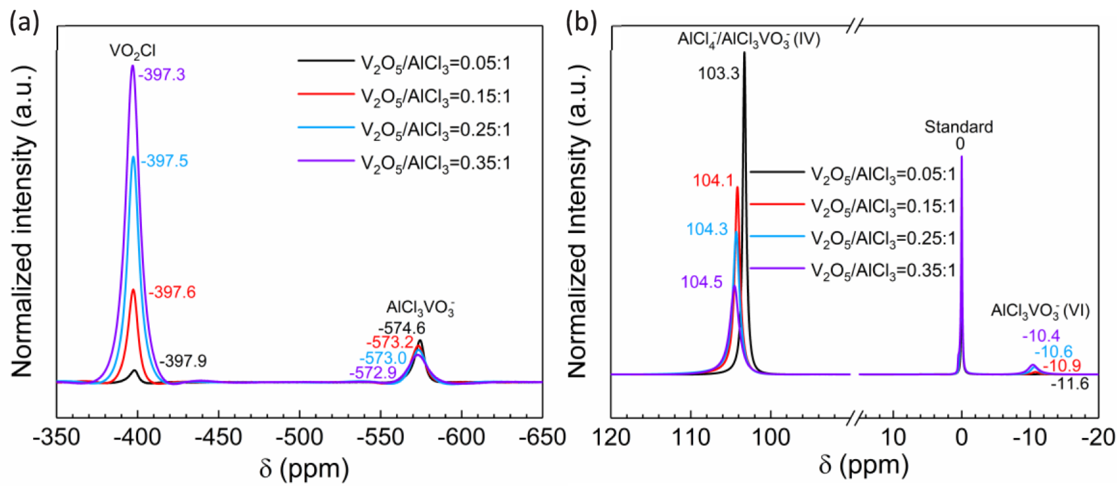

Figure 5. Liquid-state (a) ^{51}V NMR and (b) ^{27}Al NMR spectra of the Lewis neutral $AlCl_3$-[EMIm]Cl electrolyte after reaction with V_2O_5 at different $V_2O_5/AlCl_3$ molar ratios.

430 cm^{-1} in the spectrum of the pristine electrolyte are attributed to the Al−Cl−Al symmetric stretch and terminal Al−Cl symmetric stretch of $Al_2Cl_7^-$, respectively.[54] Furthermore, the small peak at 350 cm^{-1} is correlated to the symmetric Cl−Al−Cl stretch of $AlCl_4^-$ from the dynamic exchange between $Al_2Cl_7^-$ and $AlCl_4^-$ in Reaction 4.[55] After the reaction with V_2O_5, the intensity of the $AlCl_4^-$ peak at 350 cm^{-1} increased significantly with a simultaneous decrease of the $Al_2Cl_7^-$ peaks at 310 and 430 cm^{-1}, indicating the consumption of $Al_2Cl_7^-$ by its reaction with V_2O_5. An intensive new peak appears at 408 cm^{-1} after the reaction, which can be attributed to the vibrational modes of $VOCl_3$. This peak assignment is supported by the Raman spectrum of the commercial $VOCl_3$ displayed in Figure 3b, from which three additional peaks at 243, 498, and 1030 cm^{-1} in the spectrum after the reaction with V_2O_5 can be assigned to the vibrational modes of $VOCl_3$. The $VOCl_3$ peak at 498 cm^{-1} is relatively weak and thus is buried within the noise of the spectrum background. In addition, the $VOCl_3$ peak at 243 cm^{-1} overlaps with the peak indexed to the out-of-plane stretching and wagging of the methyl-N group of $[EMIm]^+$.[54] The $VOCl_3$ peak assignment is also strongly supported by the calculated Raman spectrum of $VOCl_3$ based on density functional theory (DFT) (Figure S6 and Table S2, Supporting Information). The Raman spectrum of the Lewis acidic $AlCl_3$-[EMIm]Cl electrolyte after the reaction at room temperature confirms the identical products (Figure S7, Supporting Information).

Based on the electrochemical and spectroscopic analyses discussed above, we propose the following reaction between V_2O_5 and $Al_2Cl_7^-$:

$$V_2O_5 + 2Al_2Cl_7^- \rightarrow 2VOCl_3 + 2AlCl_4^- + Al_2O_3(s) \qquad (5)$$

To study the potential chemical reaction between V_2O_5 and the Lewis neutral $AlCl_4^-$, V_2O_5 was reacted with the $AlCl_3$-[EMIm]Cl (molar ratio 1:1) electrolyte with four different $V_2O_5/AlCl_3$ molar ratios at 0.05:1, 0.15:1, 0.25:1, and 0.35:1. The reaction at the 0.05:1 ratio was performed at room temperature, and the other ratios were performed at 70 °C to expedite the reaction. In all reactions, V_2O_5 was completely dissolved with a distinct color change and no precipitation (Figure S8 in Supporting Information). CV of the Lewis neutral $AlCl_3$-[EMIm]Cl electrolyte was performed before and after the reaction. To clearly illustrate the change of electrochemical properties induced by the reaction with V_2O_5, the CV scan was performed in two separate electrochemical windows: −1.0 to 1.5 V and 1.5 to 3.5 V vs Al, respectively. As shown in Figure 4a, the CV of the pristine Lewis neutral electrolyte between −1.0 and 1.5 V exhibits no

DOI: 10.1021/acs.chemmater.9b01556
Chem. Mater. 2019, 31, 7238−7247

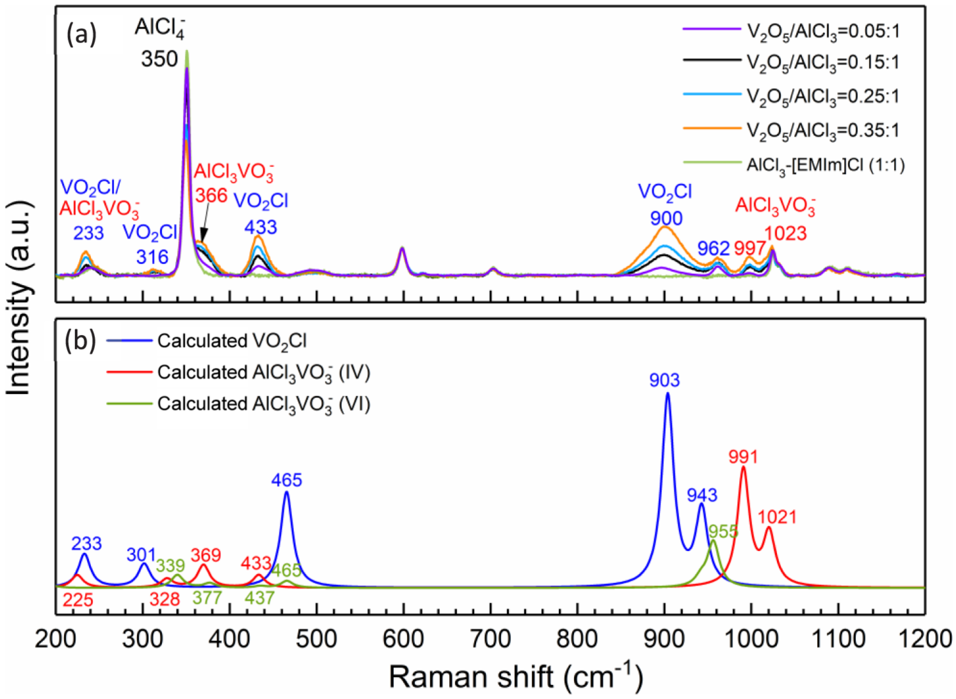

Figure 6. (a) Raman spectra of the Lewis neutral $AlCl_3$-[EMIm]Cl (molar ratio 1:1) electrolyte before and after reaction with V_2O_5; (b) DFT-calculated Raman spectra of VO_2Cl and $AlCl_3VO_3^-$.

Al electrodeposition-stripping behavior as expected, since $AlCl_4^-$ is known to be inert toward electrochemical reduction.[24] Interestingly, after the reaction with V_2O_5, a pair of redox peaks appeared in all electrolytes. The electrochemical potential of this redox pair seems to decrease with an increasing $V_2O_5/AlCl_3$ molar ratio. We show below that this electrochemical activity is not attributed to reversible electro-deposition of Al metal; instead, it is due to electrochemical V^{5+}/V^{2+} redox reactions associated with the reaction products. In the electrochemical window between 1.5 and 3.5 V shown in Figure 4b, the CV of the pristine Lewis neutral electrolyte shows an irreversible oxidization peak with onset at 2.6 V, which is due to chlorine evolution via electrochemical oxidation of $AlCl_4^-$ according to Reaction 6:[56]

$$4AlCl_4^- - 2e^- \rightarrow 2Al_2Cl_7^- + Cl_2 \quad (6)$$

After the reaction with V_2O_5, the oxidation peaks are significantly reduced, particularly for the two higher $V_2O_5/AlCl_3$ molar ratios at 0.25:1 and 0.35:1, at which the oxidation of $AlCl_4^-$ almost completely diminishes. This observation clearly establishes the decrease of the concentration of $AlCl_4^-$ in the electrolyte due to the reaction with V_2O_5.

To identify the reaction products, liquid-state ^{51}V and ^{27}Al NMR, Raman spectroscopy, and DFT-based calculations were performed. Liquid-state ^{51}V NMR spectra of the Lewis neutral electrolytes after the reaction with V_2O_5 are shown in Figure 5a (full spectra in Supporting Information, Figure S9), where the ^{51}V peak positions and integrals are normalized by the reference (mixture of 90 vol % $VOCl_3$ and 10 vol % C_6D_6). The peak at ca. −574 ppm is attributed to species containing a metavanadate VO_3^- anion based on previous reports.[57,58] Based on the presence of VO_3^-, we speculate that the other V-containing species, represented by the NMR peak at ca. −397 ppm, is dioxovanadium(V) chloride (VO_2Cl) from the splitting of V_2O_5. The liquid-state ^{27}Al NMR spectra in Figure 5b (full spectra in Supporting Information, Figure S9) are also normalized by the reference (1 M $AlCl_3$ in D_2O). The ^{27}Al NMR spectra indicate the generation of a new Al-containing species represented by the signal at ca. −11 ppm. This new Al-containing species may be associated with the metavanadate VO_3^- anionic species identified by liquid-state ^{51}V NMR. Thus, we hypothesize this species is $AlCl_3VO_3^-$, a new compound composed of $AlCl_3$ coordinated with VO_3^-. Furthermore, the Al in the proposed $AlCl_3VO_3^-$ at ca. −11 ppm should be in a 6-coordinated environment ($AlCl_3VO_3^-$(VI)) based on its chemical shift.[59]

The electrolyte after the reaction was further characterized with Raman spectroscopy and compared with the pristine Lewis neutral electrolyte. As shown in Figure 6a, the peak at 350 cm^{-1} in the Raman spectrum of the pristine electrolyte (green curve) is attributed to the $AlCl_4^-$ anion, and the rest of the peaks are attributed to the $[EMIm]^+$ cation. After the reaction with V_2O_5, the peak intensity of $AlCl_4^-$, normalized by the $[EMIm]^+$ peak at 600 cm^{-1}, clearly decreases with an increasing $V_2O_5/AlCl_3$ ratio, indicating the consumption of $AlCl_4^-$. Furthermore, new peaks emerge at 977, 962, 900, 433, 366, 316, and 233 cm^{-1}. To assign these new peaks, the Raman spectrum of VO_2Cl was first calculated using VASP, Phonopy, and the Phonopy-Spectroscopy package with the Raman shift corrected by considering the Coulombic interactions from the $[EMIm]^+$ cations (details in Supporting Information Table S3 and Figures S10 and S11). The calculated Raman spectrum of VO_2Cl in Figure 6b (blue curve) agrees well with the experimental results, thus confirming VO_2Cl as one of the reaction products between V_2O_5 and $AlCl_4^-$. The Raman shift and vibrational modes assigned to the VO_2Cl spectrum are summarized in Table 1.

The calculation of the Raman spectrum of $AlCl_3VO_3^-$ indicates that the 6-coordinated $AlCl_3VO_3^-$(VI) is a metastable state, and the most stable state is the 4-coordinated $AlCl_3VO_3^-$(IV). Raman spectra of both structures were

DOI: 10.1021/acs.chemmater.9b01556
Chem. Mater. 2019, 31, 7238−7247

Table 1. VO_2Cl Raman Vibrational Modes and Corresponding Shifts from DFT Calculations

vibrational mode	Raman shift (cm^{-1})
VO_2 asymmetric stretching	943
VO_2 symmetric stretching	903
V−Cl stretching with weak VO_2 bending	465
VO_2 bending with weak V−Cl stretching	301
VO_2 rocking with weak V−Cl rocking	233

calculated and are plotted in Figure 6b, and the vibrational modes and Raman shift assigned to both $AlCl_3VO_3^-$ structures are summarized in Tables 2 and 3. The calculated Raman spectra of $AlCl_3VO_3^-$ agree very well with the experimental results. We hypothesize that $AlCl_3VO_3^-$(IV) and $AlCl_3VO_3^-$(VI) coexist as products by establishing a dynamic exchange, which is supported by the ^{27}Al NMR spectra in Figure 5b: the chemical shift of the 4-coordinated $AlCl_3VO_3^-$(IV) coincides with that of $AlCl_4^-$ (in which Al is also 4-coordinated). The intensity change of the ^{27}Al NMR signals with increasing $V_2O_5/AlCl_3$ ratio (i.e., increasing intensity at ca. −11 ppm accompanied by decreasing intensity at ca. 104 ppm) is also consistent with this hypothesis. Based on the analysis described above, we propose the reaction between V_2O_5 and the Lewis neutral $AlCl_4^-$ as Scheme 1.

Table 2. Four-Coordinated $AlCl_3VO_3^-$(IV) Raman Vibrational Modes and Corresponding Shifts from DFT Calculations

vibrational mode	Raman shift (cm^{-1})
VO_2 asymmetric stretching	1021
VO_2 symmetric stretching	991
V−O−Al symmetric stretching	433
VO_2 bending with V−Cl stretching	369
VO_2 wagging with V−Cl stretching	328
V−O−Al rocking	225

Table 3. Six-Coordinated $AlCl_3VO_3^-$(VI) Raman Vibrational Modes and Corresponding Shifts from DFT Calculations

vibrational mode	Raman shift (cm^{-1})
VO_2 asymmetric stretching	955
Al−Cl stretching	465
VO_3 wagging	437
VO_2 bending	377
Cl_3−Al−O_3 asymmetrical stretching	339

Scheme 1. (top) Proposed Reaction Mechanism between V_2O_5 and $AlCl_4^-$ To Produce $AlCl_3VO_3^-$ and VO_2Cl and (bottom) Proposed Dynamic Exchange between 4-Coordinated and 6-Coordinated $AlCl_3VO_3^-$

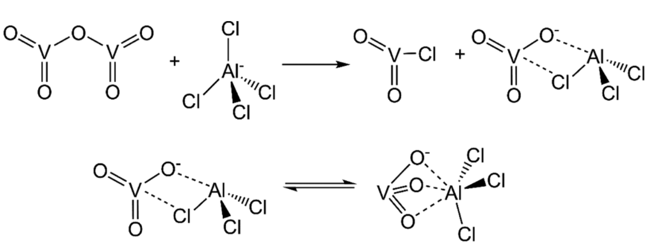

To better understand the bonding characteristics of $AlCl_3VO_3^-$(IV), $AlCl_3VO_3^-$(VI), and VO_2Cl, a Bader charge analysis and electron localization function (ELF) analysis were performed (details in Supporting Information, Tables S4−S5 and Figures S12−S18). In both structures of $AlCl_3VO_3^-$, the bonds of V−O, Al−O, Al−Cl, and V−Cl (4-coordinated structure only) are all dominantly covalent with finite ionic character. Through a similar ELF analysis, it is concluded that all bonds in the VO_2Cl molecule are also covalent. According to the Bader charge analysis of the 4-coordinated $AlCl_3VO_3^-$(IV) structure, the two O atoms with double bond to V have an equal negative charge of −0.78 e, which is lower than the negative charge carried by the O atom with the single bond (−1.25 e). On the other hand, in the 6-coordinated $AlCl_3VO_3^-$(VI) structure, all three O atoms have an equal negative charge of −1.16 e.

These V-containing compounds are likely responsible for the electrochemical activity of the Lewis neutral electrolyte, shown in Figure 4a, after the reaction with V_2O_5. The change of the redox potential at different $V_2O_5/AlCl_3$ ratios may be related to the relative concentration of these compounds. To probe the mechanism of the observed electrochemical reaction, we performed chronoamperometry deposition (−1.0 V vs Al for 40 h) on a Ta working electrode in the Lewis neutral electrolyte after the reaction with V_2O_5 ($V_2O_5/AlCl_3$ = 0.25:1). Figure 7a displays the chronoamperometric current vs time with a stable current of −0.03 mA cm^{-2}. The SEM image after chronoamperometry in Figure 7b shows cluster-like particles deposited on the Ta substrate. The EDX analysis indicates these particles contain elements including Al, V, and Cl (full EDX mapping and spectra are in Supporting Information, Figure S19). To identify the oxidation state of these elements, the surface of the deposited particles is analyzed with XPS. The Cl 2p XPS spectrum indicates the existence of metal chlorides in the deposit (Figure S20, Supporting Information). The Al 2p XPS spectrum in Figure 7c clearly demonstrates that the Al content in the deposit is not metallic and is instead likely to be aluminum oxide.[60,61] More interestingly, the V 2p XPS spectrum in Figure 7d shows a pair of peaks at 516.7 eV (V $2p_{3/2}$) and 524.1 eV (V $2p_{1/2}$), which are assigned to V^{5+}, while another pair of peaks at 514.1 eV (V $2p_{3/2}$) and 521.5 eV (V $2p_{1/2}$) are assigned to V^{2+}.[62] This result is strong evidence that certain V-containing species are reduced during the chronoamperometry. The reversible CV peaks in Figure 4a are attributed to the redox reactions between V^{5+} and V^{2+}, although determination of the exact electrochemical reaction is beyond the scope of this work. The electrochemical activity of the V-containing products from the reaction with V_2O_5 raises further questions about the interpretation of rechargeable Al−V_2O_5 batteries that use $AlCl_3$-[EMIm]Cl electrolytes (typical molar ratios range from 1.1 to 1.7), which contain both $AlCl_4^-$ and $Al_2Cl_7^-$ species.

■ CONCLUSIONS

Our investigation on the chemical compatibility between V_2O_5 and $AlCl_3$-[EMIm]Cl ionic liquid electrolytes establishes unambiguously that V_2O_5 chemically reacts with both Lewis acidic $Al_2Cl_7^-$ and Lewis neutral $AlCl_4^-$ anions. Spectroscopic, electrochemical, and theoretical analyses reveal that the reaction products between V_2O_5 and $Al_2Cl_7^-$ are $VOCl_3$ and amorphous Al_2O_3. Similarly, the reaction products between V_2O_5 and $AlCl_4^-$ are identified as VO_2Cl and $AlCl_3VO_3^-$ with both 4-coordinated and 6-coordinated structures; these soluble

DOI: 10.1021/acs.chemmater.9b01556
Chem. Mater. 2019, 31, 7238−7247

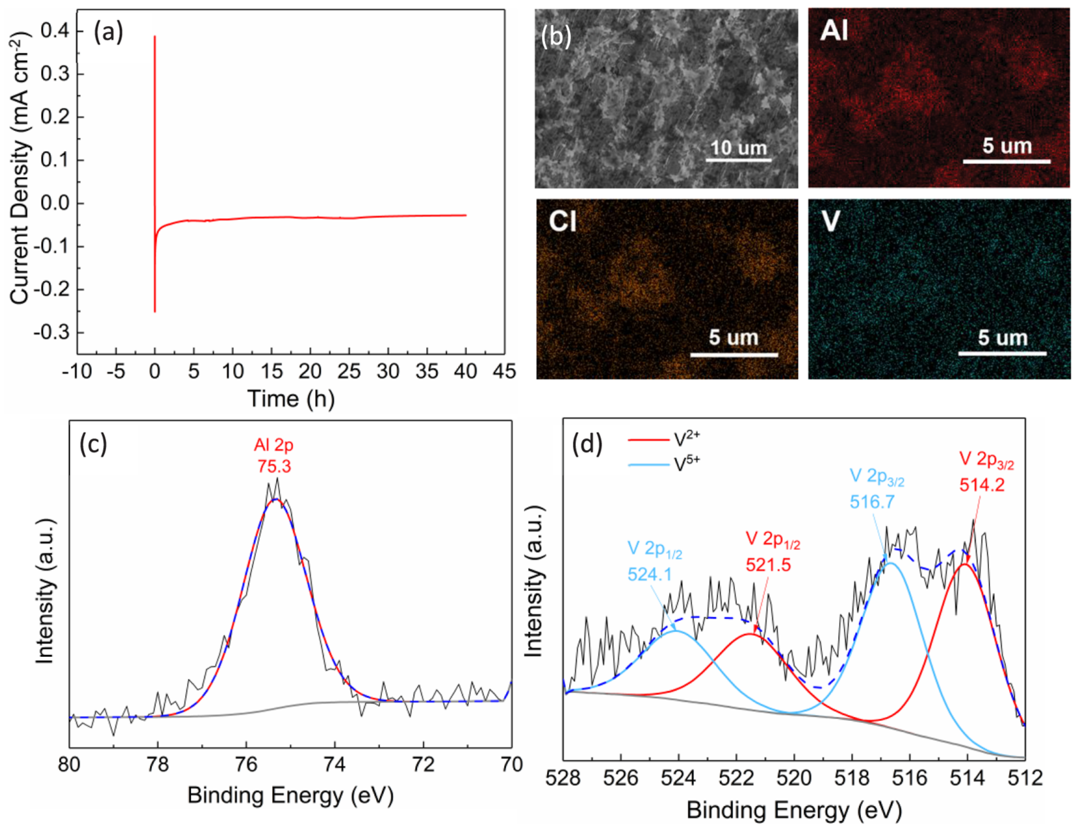

Figure 7. (a) Chronoamperometric current vs time at −1.0 V vs Al on a Ta working electrode; (b) SEM image and elemental mapping; and (c) Al 2p and (d) V 2p XPS spectra of the deposit from the Lewis neutral $AlCl_3$-[EMIm]Cl electrolyte after reaction with V_2O_5 (molar ratio $V_2O_5/AlCl_3$ = 0.25:1).

products are furthermore electrochemically active, exhibiting reversible redox reactions between V^{5+} and V^{2+} oxidation states. It is clear that V_2O_5 is not a chemically stable positive electrode material for rechargeable Al batteries using chloroaluminate ionic liquid electrolytes, regardless of Lewis acidity. Although an Al−V_2O_5 cell may appear to have electrochemical performance in terms of capacity and cyclability, researchers must be cautious when identifying the origin of the electrochemical reactions. Our investigation also raises the question of the chemical stability of other Al-ion positive electrode materials in chloroaluminate ionic liquid electrolytes.

■ ASSOCIATED CONTENT

Supporting Information

The Supporting Information is available free of charge on the ACS Publications website at DOI: 10.1021/acs.chemmater.9b01556.

Digital images of electrolytes before and after reaction with V_2O_5, XRD pattern, solid-state ^{51}V NMR, and solid-state ^{27}Al NMR parameters of each Al coordination environment in the precipitate from the reaction between V_2O_5 and the Lewis acidic electrolyte, liquid-state ^{27}Al and ^{51}V NMR spectra of the reaction products between V_2O_5 and the Lewis neutral electrolyte, DFT-computed Raman spectra and analyses of reaction products, computational analyses of bonding characteristics of the reaction products, full EDX mapping and spectra, and Cl 2p XPS of the deposit on Ta (PDF)

■ AUTHOR INFORMATION

Corresponding Authors

*(J.G.) E-mail: jguo@engr.ucr.edu.
*(R.J.M.) E-mail: rmessinger@ccny.cuny.edu.

ORCID

Jian Zhang: 0000-0003-0356-7611
Bryan M. Wong: 0000-0002-3477-8043
Robert J. Messinger: 0000-0002-5537-3870
Juchen Guo: 0000-0001-9829-1202

Notes

The authors declare no competing financial interest.

■ ACKNOWLEDGMENTS

X.W., J.Z., and J.G. acknowledge the financial support from U.S. National Science Foundation (NSF) CAREER program though Grant Number CBET-1751929. R.J.M. and A.J. acknowledge support from the NSF CAREER program (Grant CBET-1847522). XPS work was performed at the UC Irvine Materials Research Institute (IMRI) using instrumentation funded in part by the National Science Foundation Major Research Instrumentation Program under Grant No. CHE-1338173. NMR measurements were performed at the Analytical Chemistry Instrumentation Facility at UCR, funded in part by the NSF under Grant Number CHE-1626673, as well as the City University of New York Advanced Science Research Center (CUNY ASRC) NMR facility. B.S. acknowledges the Swedish Research council (Grants No. 2017-05447 and 2016-05366) for financial support. The calculations were performed on resources provided by the Swedish

DOI: 10.1021/acs.chemmater.9b01556
Chem. Mater. 2019, 31, 7238−7247

National Infrastructure for Computing (SNIC) at HPC2N under the project SNIC 2018/2-51.

REFERENCES

(1) Das, S. K.; Mahapatra, S.; Lahan, H. Aluminium-ion batteries: developments and challenges. *J. Mater. Chem. A* **2017**, *5* (14), 6347–6367.

(2) Elia, G. A.; Marquardt, K.; Hoeppner, K.; Fantini, S.; Lin, R.; Knipping, E.; Peters, W.; Drillet, J. F.; Passerini, S.; Hahn, R. An overview and future perspectives of aluminum batteries. *Adv. Mater.* **2016**, *28* (35), 7564–7579.

(3) Yu, Z.; Jiao, S.; Li, S.; Chen, X.; Song, W.-L.; Teng, T.; Tu, J.; Chen, H.-S.; Zhang, G.; Fang, D.-N. Flexible Stable Solid-State Al-Ion Batteries. *Adv. Funct. Mater.* **2019**, *29*, 1806799.

(4) Nakayama, Y.; Senda, Y.; Kawasaki, H.; Koshitani, N.; Hosoi, S.; Kudo, Y.; Morioka, H.; Nagamine, M. Sulfone-based electrolytes for aluminium rechargeable batteries. *Phys. Chem. Chem. Phys.* **2015**, *17* (8), 5758–66.

(5) Abbott, A. P.; Qiu, F.; Abood, H. M.; Ali, M. R.; Ryder, K. S. Double layer, diluent and anode effects upon the electrodeposition of aluminium from chloroaluminate based ionic liquids. *Phys. Chem. Chem. Phys.* **2010**, *12* (8), 1862–1872.

(6) Zhang, Q.; Wang, Q.; Zhang, S.; Lu, X. Effect of nicotinamide on electrodeposition of Al from aluminium chloride ($AlCl_3$)-1-butyl-3-methylimidazolium chloride ([Bmim]Cl) ionic liquids. *J. Solid State Electrochem.* **2014**, *18* (1), 257–267.

(7) Wang, Q.; Chen, B.; Zhang, Q.; Lu, X.; Zhang, S. Aluminum Deposition from Lewis Acidic 1-Butyl-3-Methylimidazolium Chloroaluminate Ionic Liquid ([Bmim]Cl/$AlCl_3$) Modified with Methyl Nicotinate. *ChemElectroChem* **2015**, *2* (11), 1794–1798.

(8) Kamath, G.; Narayanan, B.; Sankaranarayanan, S. K. Atomistic origin of superior performance of ionic liquid electrolytes for Al-ion batteries. *Phys. Chem. Chem. Phys.* **2014**, *16* (38), 20387–20391.

(9) Jiang, T.; Chollier Brym, M. J.; Dubé, G.; Lasia, A.; Brisard, G. M. Electrodeposition of aluminium from ionic liquids: Part I—electrodeposition and surface morphology of aluminium from aluminium chloride ($AlCl_3$)−1-ethyl-3-methylimidazolium chloride ([EMIm]Cl) ionic liquids. *Surf. Coat. Technol.* **2006**, *201* (1–2), 1–9.

(10) Pradhan, D.; Reddy, R. G. Mechanistic study of Al electrodeposition from EMIC−$AlCl_3$ and BMIC−$AlCl_3$ electrolytes at low temperature. *Mater. Chem. Phys.* **2014**, *143* (2), 564–569.

(11) Lee, J. J.; Bae, I. T.; Scherson, D. A.; Miller, B.; Wheeler, K. A. Underpotential deposition of aluminum and alloy formation on polycrystalline gold electrodes from $AlCl_3$/EMIC room-temperature molten salts. *J. Electrochem. Soc.* **2000**, *147* (2), 562–566.

(12) Reed, L. D.; Menke, E. The Roles of V_2O_5 and Stainless Steel in Rechargeable Al-ion Batteries. *J. Electrochem. Soc.* **2013**, *160* (6), A915–A917.

(13) Rong, Z.; Malik, R.; Canepa, P.; Sai Gautam, G.; Liu, M.; Jain, A.; Persson, K.; Ceder, G. Materials Design Rules for Multivalent Ion Mobility in Intercalation Structures. *Chem. Mater.* **2015**, *27* (17), 6016–6021.

(14) Gao, T.; Li, X.; Wang, X.; Hu, J.; Han, F.; Fan, X.; Suo, L.; Pearse, A. J.; Lee, S. B.; Rubloff, G. W.; et al. A Rechargeable Al/S Battery with an Ionic-Liquid Electrolyte. *Angew. Chem.* **2016**, *128*, 10052–10055.

(15) Huang, X.; Liu, Y.; Liu, C.; Zhang, J.; Noonan, O.; Yu, C. Rechargeable aluminum-selenium batteries with high capcacity. *Chem. Sci.* **2018**, *9*, 5178–5182.

(16) Zhang, X.; Jiao, S.; Tu, J.; Song, W.-L.; Xiao, X.; Li, S.; Wang, M.; Lei, H.; Tian, D.; Chen, H.; et al. Rechargeable ultrahigh-capacity tellurium-aluminum batteries. *Energy Environ. Sci.* **2019**, *12*, 1918–1927.

(17) Takami, N.; Koura, N. Electrochemical Behavior of FeS_2 Cathodes for Aluminum Secondary Cells around 100° C. *J. Electrochem. Soc.* **1993**, *140* (4), 928–932.

(18) Wang, W.; Jiang, B.; Xiong, W.; Sun, H.; Lin, Z.; Hu, L.; Tu, J.; Hou, J.; Zhu, H.; Jiao, S. A new cathode material for super-valent battery based on aluminium ion intercalation and deintercalation. *Sci. Rep.* **2013**, *3*, 3383.

(19) Geng, L.; Lv, G.; Xing, X.; Guo, J. Reversible electrochemical intercalation of aluminum in Mo_6S_8. *Chem. Mater.* **2015**, *27* (14), 4926–4929.

(20) Wang, S.; Yu, Z.; Tu, J.; Wang, J.; Tian, D.; Liu, Y.; Jiao, S. A Novel Aluminum-Ion Battery: Al/$AlCl_3$-[EMIm]Cl/Ni_3S_2@Graphene. *Adv. Energy Mater.* **2016**, *6* (13), 1600137.

(21) Yu, Z.; Kang, Z.; Hu, Z.; Lu, J.; Zhou, Z.; Jiao, S. Hexagonal NiS nanobelts as advanced cathode materials for rechargeable Al-ion batteries. *Chem. Commun.* **2016**, *52* (68), 10427–10430.

(22) Wang, S.; Jiao, S.; Wang, J.; Chen, H. S.; Tian, D.; Lei, H.; Fang, D. N. High-Performance Aluminum-Ion Battery with CuS@C Microsphere Composite Cathode. *ACS Nano* **2017**, *11* (1), 469–477.

(23) Geng, L.; Scheifers, J. P.; Fu, C.; Zhang, J.; Fokwa, B. P. T.; Guo, J. Titanium Sulfides as Interclation-Type Catode materials for Rechargeable Aluminum Batteries. *ACS Appl. Mater. Interfaces* **2017**, *9*, 21251–21257.

(24) Geng, L.; Scheifers, J. P.; Zhang, J.; Bozhilov, K. N.; Fokwa, B. P. T.; Guo, J. Crystal Structure Transfomation in Chevrel Phase Mo6S8 Induced by Aluminum Intercalation. *Chem. Mater.* **2018**, *30*, 8420–8425.

(25) Gu, S.; Wang, H.; Wu, C.; Bai, Y.; Li, H.; Wu, F. Confirming reversible Al^{3+} storage mechanism through intercalation of Al^{3+} into V_2O_5 nanowires in a rechargeable aluminum battery. *Energy Storage Materials* **2017**, *6*, 9–17.

(26) Wang, H.; Gu, S.; Bai, Y.; Chen, S.; Zhu, N.; Wu, C.; Wu, F. Anion-effects on electrochemical properties of ionic liquid electrolytes for rechargeable aluminum batteries. *J. Mater. Chem. A* **2015**, *3* (45), 22677–22686.

(27) Ferrara, C.; Dall'Asta, V.; Berbenni, V.; Quartarone, E.; Mustarelli, P. Physicochemical Characterization of $AlCl_3$−1-Ethyl-3-methylimidazolium Chloride Ionic Liquid Electrolytes for Aluminum Rechargeable Batteries. *J. Phys. Chem. C* **2017**, *121* (48), 26607–26614.

(28) Wang, H.; Bi, X.; Bai, Y.; Wu, C.; Gu, S.; Chen, S.; Wu, F.; Amine, K.; Lu, J. Open-Structured $V_2O_5{\cdot}nH_2O$ Nanoflakes as Highly Reversible Cathode Material for Monovalent and Multivalent Intercalation Batteries. *Adv. Energy Mater.* **2017**, *7* (14), 1602720.

(29) Wang, H.; Bai, Y.; Chen, S.; Luo, X.; Wu, C.; Wu, F.; Lu, J.; Amine, K. Binder-free V_2O_5 cathode for greener rechargeable aluminum battery. *ACS Appl. Mater. Interfaces* **2015**, *7* (1), 80–84.

(30) Chiku, M.; Takeda, H.; Matsumura, S.; Higuchi, E.; Inoue, H. Amorphous vanadium oxide/carbon composite positive electrode for rechargeable aluminum battery. *ACS Appl. Mater. Interfaces* **2015**, *7* (44), 24385–24389.

(31) Wang, Q.; Zhang, Q.; Lu, X.; Zhang, S. Electrodeposition of Al from chloroaluminate ionic liquids with different cations. *Ionics* **2017**, *23* (9), 2449–2455.

(32) Pan, A. Q.; Zhang, J. G.; Nie, Z. M.; Cao, G. Z.; Arey, B. W.; Li, G. S.; Liang, S. Q.; Liu, J. Facile synthesized nanorod structured vanadium pentoxide for high-rate lithium batteries. *J. Mater. Chem.* **2010**, *20* (41), 9193–9199.

(33) Kresse, G.; Furthmüller, J. Efficient iterative schemes for ab initio total-energy calculations using a plane-wave basis set. *Phys. Rev. B: Condens. Matter Mater. Phys.* **1996**, *54* (16), 11169–11186.

(34) Kresse, G.; Hafner, J. Ab initio molecular dynamics for liquid metals. *Phys. Rev. B: Condens. Matter Mater. Phys.* **1993**, *47* (1), 558–561.

(35) Kresse, G.; Joubert, D. From ultrasoft pseudopotentials to the projector augmented-wave method. *Phys. Rev. B: Condens. Matter Mater. Phys.* **1999**, *59* (3), 1758–1775.

(36) Blöchl, P. E. Projector augmented-wave method. *Phys. Rev. B: Condens. Matter Mater. Phys.* **1994**, *50* (24), 17953–17979.

(37) Perdew, J. P.; Burke, K.; Ernzerhof, M. Generalized Gradient Approximation Made Simple. *Phys. Rev. Lett.* **1996**, *77* (18), 3865–3868.

(38) Elsässer, C.; Fähnle, M.; Chan, C. T.; Ho, K. M. Density-functional energies and forces with Gaussian-broadened fractional

DOI: 10.1021/acs.chemmater.9b01556
Chem. Mater. 2019, 31, 7238–7247

occupations. *Phys. Rev. B: Condens. Matter Mater. Phys.* **1994**, *49* (19), 13975−13978.
(39) Monkhorst, H. J.; Pack, J. D. Special points for Brillouin-zone integrations. *Phys. Rev. B* **1976**, *13* (12), 5188−5192.
(40) Togo, A.; Tanaka, I. First principles phonon calculations in materials science. *Scr. Mater.* **2015**, *108*, 1−5.
(41) Skelton, J. M.; Burton, L. A.; Jackson, A. J.; Oba, F.; Parker, S. C.; Walsh, A. Lattice dynamics of the tin sulphides SnS_2, SnS and Sn_2S_3: vibrational spectra and thermal transport. *Phys. Chem. Chem. Phys.* **2017**, *19* (19), 12452−12465.
(42) Savin, A.; Nesper, R.; Wengert, S.; Fässler, T. F. ELF: The electron localization function. *Angew. Chem., Int. Ed. Engl.* **1997**, *36* (17), 1808−1832.
(43) Henkelman, G.; Arnaldsson, A.; Jónsson, H. A fast and robust algorithm for Bader decomposition of charge density. *Comput. Mater. Sci.* **2006**, *36* (3), 354−360.
(44) Tang, W.; Sanville, E.; Henkelman, G. A grid-based Bader analysis algorithm without lattice bias. *J. Phys.: Condens. Matter* **2009**, *21* (8), No. 084204.
(45) Schaltin, S.; Ganapathi, M.; Binnemans, K.; Fransaer, J. Modeling of aluminium deposition from chloroaluminate ionic liquids. *J. Electrochem. Soc.* **2011**, *158* (10), D634−D639.
(46) Davis, M. F.; Jura, M.; Leung, A.; Levason, W.; Littlefield, B.; Reid, G.; Webster, M. Synthesis, chemistry and structures of complexes of the dioxovanadium(V) halides VO_2F and VO_2Cl. *Dalton Trans.* **2008**, No. 44, 6265−73.
(47) Slebodnick, C.; Pecoraro, V. L. Solvent effects on 51V NMR chemical shifts: characterization of vanadate and peroxovanadate complexes in mixed water/acetonitrile solvent. *Inorg. Chim. Acta* **1998**, *283* (1), 37−43.
(48) Kraus, H.; Prins, R.; Kentgens, A. A ^{27}Al MQMAS and Off-Resonance Nutation NMR Investigation of Mo− P/γ-Al_2O_3 Hydrotreating Catalyst Precursors. *J. Phys. Chem.* **1996**, *100* (40), 16336−16345.
(49) Iuga, D.; Simon, S.; De Boer, E.; Kentgens, A. A nuclear magnetic resonance study of amorphous and crystalline lanthanum-aluminates. *J. Phys. Chem. B* **1999**, *103* (36), 7591−7598.
(50) Neuville, D. R.; Cormier, L.; Massiot, D. Al environment in tectosilicate and peraluminous glasses: A 27Al MQ-MAS NMR, Raman, and XANES invesitgation. *Geochim. Cosmochim. Acta* **2004**, *68* (24), 5071−5079.
(51) Lee, S. K.; Park, S. Y.; Yi, Y. S.; Moon, J. Structure and Disorder in Amorphous Alumina Thin Films: Insights from High-Resolution Solid-State NMR. *J. Phys. Chem. C* **2010**, *114* (32), 13890−13894.
(52) O'Dell, L. A.; Savin, S. L.; Chadwick, A. V.; Smith, M. E. A ^{27}Al MAS NMR study of a sol-gel produced alumina: Identification of the NMR parameters of the theta-Al_2O_3 transition alumina phase. *Solid State Nucl. Magn. Reson.* **2007**, *31* (4), 169−73.
(53) Wischert, R.; Florian, P.; Copéret, C.; Massiot, D.; Sautet, P. Visibility of Al Surface Sites of γ-Alumina: A Combined Computational and Experimental Point of View. *J. Phys. Chem. C* **2014**, *118* (28), 15292−15299.
(54) Katsyuba, S. A.; Dyson, P. J.; Vandyukova, E. E.; Chernova, A. V.; Vidiš, A. Molecular Structure, Vibrational Spectra, and Hydrogen Bonding of the Ionic Liquid 1-Ethyl-3-methyl-1H-imidazolium Tetrafluoroborate. *Helv. Chim. Acta* **2004**, *87* (10), 2556−2565.
(55) Bertasi, F.; Hettige, C.; Sepehr, F.; Bogle, X.; Pagot, G.; Vezzù, K.; Negro, E.; Paddison, S. J.; Greenbaum, S. G.; Vittadello, M.; Di Noto, V. A key concept in magnesium secondary battery electrolytes. *ChemSusChem* **2015**, *8* (18), 3069−3076.
(56) Carlin, R. T.; Crawford, W.; Bersch, M. Nucleation and Morphology Studies of Aluminum Deposited from an Ambient-Temperature Chloroaluminate Molten Salt. *J. Electrochem. Soc.* **1992**, *139* (10), 2720−2727.
(57) Bell, R.; Castleman, A.; Thorn, D. Vanadium oxide complexes in room-temperature chloroaluminate molten salts. *Inorg. Chem.* **1999**, *38* (25), 5709−5715.
(58) Mason, J. *Multinuclear NMR*; Plenum Press: New York, 2012.
(59) Akitt, J. W. Multinuclear studies of aluminium compounds. *Prog. Nucl. Magn. Reson. Spectrosc.* **1989**, *21* (1−2), 1−149.
(60) Xin, Y.; Huo, K.; Hu, T.; Tang, G.; Chu, P. K. Mechanical properties of Al_2O_3/Al bi-layer coated AZ91 magnesium alloy. *Thin Solid Films* **2009**, *517* (17), 5357−5360.
(61) Li, F.; Tang, H.; Anderegg, J.; Shinar, J. Fabrication and electroluminescence of double-layered organic light-emitting diodes with the Al_2O_3/Al cathode. *Appl. Phys. Lett.* **1997**, *70* (10), 1233−1235.
(62) Biesinger, M. C.; Lau, L. W. M.; Gerson, A. R.; Smart, R. S. C. Resolving surface chemical states in XPS analysis of first row transition metals, oxides and hydroxides: Sc, Ti, V, Cu and Zn. *Appl. Surf. Sci.* **2010**, *257* (3), 887−898.

DOI: 10.1021/acs.chemmater.9b01556
Chem. Mater. 2019, 31, 7238−7247